Thermal fluctuation-induced tunneling conduction through metal nanowire contacts

2008 Nanotechnology 19 365201

(http://iopscience.iop.org/0957-4484/19/36/365201)

Nanotechnology **19** (2008) 365201 (7pp) doi:10.1088/0957-4484/19/36/365201

Thermal fluctuation-induced tunneling conduction through metal nanowire contacts

Yong-Han Lin[1], **Shao-Pin Chiu**[1] **and Juhn-Jong Lin**[1,2]

[1] Institute of Physics, National Chiao Tung University, Hsinchu 30010, Taiwan
[2] Department of Electrophysics, National Chiao Tung University, Hsinchu 30010, Taiwan

E-mail: yonghanlin@gmail.com and jjlin@mail.nctu.edu.tw

Received 6 May 2008, in final form 16 June 2008
Published 25 July 2008
Online at stacks.iop.org/Nano/19/365201

Abstract

The temperature behavior of how electrons propagate through an insulating electronic contact formed at the interface between a submicron Cr/Au electrode and a metallic RuO_2 nanowire (NW) has been studied between 300 and 1 K. The NWs are typically of ∼70 nm in diameter and a few microns long. The submicron electrodes were fabricated by the standard electron-beam lithography technique. By employing the two-probe method, the electronic contact resistances, $R_c(T)$, have been determined. We found that, in general, R_c increases rapidly with decreasing temperature but eventually saturates at liquid-helium temperatures. Such a temperature behavior can be well described by a thermal fluctuation-induced tunneling (FIT) conduction process which considers the crossover feature from thermal activation conduction at high temperatures to simple elastic tunneling conduction at low temperatures. The wide applicability of this FIT model has further been established by employing metallic IrO_2 and Sn-doped In_2O_{3-x} NWs. This work demonstrates that the underlying physics for the charge transport properties of an insulating electronic contact can be well understood.

(Some figures in this article are in colour only in the electronic version)

1. Introduction

Nanoscale structures have recently become the subject of intense investigations owing to their importance for both fundamental research and potential industrial applications. Among the various nanostructures, self-assembled quasi-one-dimensional nanowires (NWs) are of particular interest, primarily due to their rich and fascinating electrical properties [1, 2]. To explore how electrons transport through these quasi-one-dimensional systems, nanofabrication techniques such as electron-beam lithography and focused ion beam deposition are often employed. Nevertheless, it is known that the fabrication of reliable electronic contacts to nanodevices is a nontrivial task. Very often, an insulating or semiconducting contact forms at the interface between a metal electrode and a nanodevice. Such an electronic contact may possess a strongly temperature dependent contact resistance, $R_c(T)$, and thus can seriously complicate the measured resistance of the NW device. Some efforts aimed at addressing this problem have been carried out in systems such as carbon nanotubes [3, 4] and semiconducting NWs [5, 6]. For instance, electronic transport properties through the contact between a metal electrode and a ZnO NW have been studied [6]. In the case of metallic NWs, although several techniques developed to improve the quality of the contacts have been reported [7, 8], the detailed electronic transport properties of an insulating contact have been scarcely addressed thus far. Since the as-grown metal NWs are often covered by a thin layer of some insulators (oxidations, contaminations, amorphous coating, etc) that is a few nanometers thick, the question of how charge transports through such a 'potential barrier' is of fundamental interest and industrial importance.

In this work, we report the temperature behavior between 300 and 1 K of insulating electronic contacts formed at the interfaces between lithographic-patterned submicron Cr/Au electrodes and single metallic NWs. The $R_c(T)$ values were determined from electrical measurements on individual NW devices by employing the two-probe, complemented with the four-probe, scheme as depicted in figures 1(a)–(c). In the four-probe method, the intrinsic NW resistance, R_s, can be

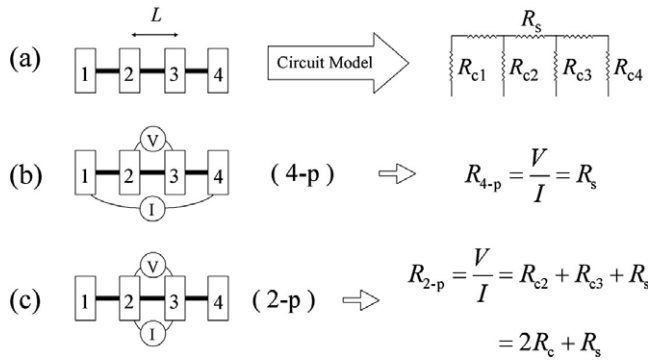

Figure 1. (a) Schematic diagram for a single NW (thick bar) with four electronic contacts on it and the equivalent circuit model. R_s denotes the intrinsic NW resistance of each segment. R_{ci} denotes the electronic contact resistance between the NW and the ith submicron electrode. (b) Four-probe and (c) two-probe measurement configurations, and the corresponding measured resistances. In (c), we assume $R_{c2} \approx R_{c3} = R_c$ (see text).

accurately determined, which is always below 1 kΩ in this study. In the two-probe method, the measured resistance R is given by $R = 2R_c + R_s$. Here the prefactor 2 is introduced to denote that there are two similar electronic contacts in series in the two-probe configuration[3]. (For simplicity, we assume that the two electronic contacts are similar, because they were fabricated simultaneously under the same conditions on the same NW.) In the case of $R \gg R_s$ (which is pertinent to this study), R_c would dominate the measured resistance, and $R \approx 2R_c$ for the whole range of experimental temperature. The measured magnitude and temperature behavior of R thus faithfully reflect the magnitude and temperature behavior of R_c. (Notice that, in the extreme case of one of the two contact resistances being sufficiently larger than the other, the measured $R(T)$ then describes the temperature behavior of a single contact resistance.) In this work, single-crystalline RuO_2 NWs, which exhibit metallic conductivity comparable with that of normal metals [9, 10], are chosen to fabricate NW devices to substantiate this idea of *experimentally quantifying* an electronic contact resistance. We found that the temperature behavior of R_c over a very wide range of temperature from 300 K down to liquid-helium temperatures can be *well* described by the thermal fluctuation-induced tunneling (FIT) conduction model proposed by Sheng and co-workers [11, 12]. As a result, the junction parameters such as the barrier height and width, which characterize an insulating electronic contact (which was modeled as a potential barrier in the FIT theory), can be explicitly inferred.

2. Experimental method

Self-assembled single-crystalline RuO_2 NWs were synthesized by the thermal evaporation method, as has been described previously [13]. The NWs used for the fabrication of two-probe devices in this work were typically 70 nm in diameter and a few micrometers long. Electrical contacts

[3] The resistances of the submicron Cr/Au electrodes are always negligibly small (∼10 Ω) compared with R_c, and hence can be ignored.

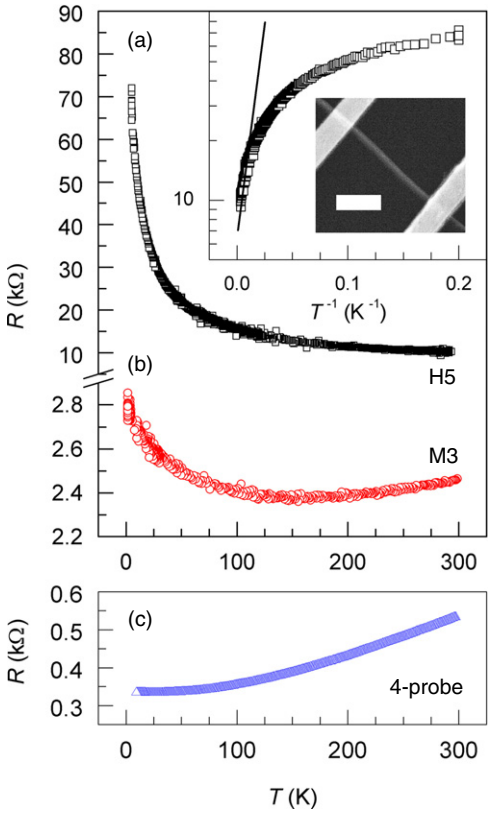

Figure 2. Resistance as a function of temperature for individual RuO_2 NW devices. (a) Two-probe result for the case $R \approx 2R_c$, (b) two-probe result for the case $R = 2R_c + R_s$, and (c) four-probe result for a 60 nm diameter NW. The inset is a replot of (a) to illustrate the variation of log R with T^{-1}, where the straight solid line indicates the thermal activation conduction. Also shown is an SEM image for a two-probe NW device fabricated with electron-beam lithography. The scale bar is 1 μm. Notice that the scales of the ordinate increase consecutively by approximately one order of magnitude from (c) to (b) to (a).

onto single NWs were fabricated by the standard electron-beam lithography technique. A Si substrate capped with a 200 nm thick SiO_2 layer was first photo-lithographically patterned with Cr/Au (10/60 nm) 'micro-electrodes' using a bi-layer photoresist process to create reverse-slope resist sidewall profiles. Several droplets of dispersed alcoholic solution containing RuO_2 NWs were dropped on the substrate. The positions of individual NWs were then determined by SEM. A spin-coated thick layer of PMMA (polymethyl methacrylate) on top of the substrate was exposed to an electron beam to produce submicron patterns. Following the thermal evaporation of Cr/Au films (≈10/90 nm), the lift-off technique was applied to generate submicron electrodes contacting the NWs. The electrodes are typically a few hundreds of nanometers wide, as explicitly listed in tables 1–3 for each device. An SEM image for a representative two-probe NW device is shown in the inset to figure 2(a).

Copper leads were attached with Ag paste to the micro-electrodes on the substrate, and the substrate was thermally anchored to a sample holder situated on a standard ^{4}He cryostat. The temperature was monitored with a calibrated silicon diode. The resistances were measured by two different

Table 1. Values of relevant parameters for seven high-resistance RuO_2 NW devices, as determined from the two-probe method. For each device, the NW resistance R_s(300 K) was determined from the four-probe method, while the junction area A was estimated from the SEM image and is given by the product of the diameter of the NW and the width of the Cr/Au electrode overlying the NW. $\rho_{c0} = \rho_c(T \to 0)$, in units of k$\Omega$ μm^2.

	R(300 K) (kΩ)	R_s(300 K) (kΩ)	R_∞ (kΩ)	T_1 (K)	T_0 (K)	A (nm^2)	w (nm)	V_0 (meV)	T_1/T_0	ρ_{c0}
H1	1.77	0.03	0.084	1396	173	400 × 650	15.7	4.1	8.07	69.2
H2	33	0.81	18.9	205	48	70 × 240	8.1	4.4	4.27	23.6
H3	33	0.33	13.6	363	104	60 × 370	6.4	4.6	3.49	9.81
H4	241	0.67	112	316	91	60 × 380	6.6	4.2	3.47	83.0
H5	10.3	0.31	8.08	87	37	70 × 570	7.0	1.7	2.35	3.39
H6	3.1	0.33	2.82	20	8.6	70 × 400	8.7	1.1	2.33	0.81
H7	25	0.81	24.7	11.9	11.7	60 × 250	4.4	0.8	1.02	1.04

Table 2. Values of relevant parameters for three moderately high-resistance RuO_2 NW devices, as determined from the two-probe method. For each device, the NW resistance R_s(300 K) was determined from the four-probe method, while the junction area A was estimated from the SEM image and is given by the product of the diameter of the NW and the width of the Cr/Au electrode overlying the NW. $\rho_{c0} = \rho_c(T \to 0)$, in units of k$\Omega$ μm^2.

	R(300 K) (kΩ)	R_s(300 K) (kΩ)	R_∞ (kΩ)	T_1 (K)	T_0 (K)	α (Ω K^{-1})	A (nm^2)	w (nm)	V_0 (meV)	T_1/T_0	ρ_{c0}
M1	1.7	0.56	1.19	52	109	1.2	70 × 410	2.0	0.85	0.48	0.06
M2	7.5	1.63	4.76	48	102	7.1	70 × 500	2.1	0.75	0.47	0.27
M3	2.5	0.53	1.86	37	90	1.4	70 × 430	1.9	0.68	0.41	0.08

Table 3. Values of relevant parameters for one IrO_2 and one ITO NW devices, as determined from the two-probe method. For each device, the NW resistance R_s(300 K) was determined from the four-probe method, while the junction area A was estimated from the SEM image and is given by the product of the diameter of the NW and the width of the Cr/Au electrode overlying the NW. $\rho_{c0} = \rho_c(T \to 0)$, in units of k$\Omega$ μm^2.

	R(300 K) (kΩ)	R_s(300 K) (kΩ)	R_∞ (kΩ)	T_1 (K)	T_0 (K)	A (nm^2)	w (nm)	V_0 (meV)	T_1/T_0	ρ_{c0}
IrO_2	4.8	0.30	2.16	364	101	90 × 480	7.5	3.5	3.60	3.42
ITO	3.6	0.12	2.62	183	284	160 × 440	2.4	1.1	0.64	0.35

methods, depending on which measurement configuration was employed. For the four-probe method, a Linear Research LR-700 AC resistance bridge was applied. For the two-probe method, the resistances were measured by utilizing a Keithley K-6430 source meter as a current source and a K-182 nanovoltmeter. For some two-probe measurements involving high device resistances, only the K-6430 source meter was used. It should be noted that, for all the results reported in this work, the resistances $R(T)$ were determined with sufficiently small bias currents (typically, a few to 10 nA) where the current–voltage (I–V) characteristics were linear. (It is also worth noting that, at low bias voltages, our I–V curves are linear even at low temperatures. However, the I–V curves can become nonlinear when the bias voltages are sufficiently high, especially at low temperatures. In this work, we shall concentrate on the low bias regime where the NW 'junctions' are ohmic and the I–V curves are linear. The nonlinearity of the I–V characteristics at high bias voltages, which will reveal the nature of (for example, elastic or inelastic [14]) electron tunneling through the barrier, is currently under experimental [15] and theoretical [16] investigations.)

3. Results and discussion

To ensure the metallic nature of our RuO_2 NWs and the applicability of the theoretical FIT model, the resistance as a function of temperature for individual NWs was first determined with the four-probe method. Figure 2(c) shows a representative result for a 60 nm diameter NW, where the resistance clearly decreases with reducing temperature. Our RuO_2 NWs have typical room-temperature resistivities of $\sim$200 $\mu\Omega$ cm [17].

In practice, the R_c of an electronic contact can be written as $R_c = \rho_c/A$, where ρ_c and A are the specific contact resistivity and the area of the contact, respectively. For a macroscopic metal–metal contact, the value of R_c is usually on the order of $\sim$1 Ω. As the area A shrinks, the magnitude of R_c may increase considerably. In our case of RuO_2 NWs, the electronic contact resistances formed between the submicron Cr/Au electrodes and the NWs usually lie between several tens and several hundreds of Ω, and depend only weakly on temperature. However, in a number of fabrications, highly resistive electronic contacts with R_c (300 K) ranging from several kΩ to several tens of kΩ have also been obtained. Figure 2(a) shows a representative two-probe result for such a high-resistance contact, where $R \approx 2R_c$ (case I). Obviously, R_c is insulating or semiconducting, i.e., the resistance increases monotonically with reducing temperature. Figure 2(b) shows a representative two-probe result for a 'moderately' high-resistance contact. In this case, $R = 2R_c + R_s$, with R_c being roughly constant around room temperature while $R_c \gg R_s$ at low temperatures (case II). Conceptually, one can envisage

the insulating contact as a tunnel junction. A single NW device in our two-probe configuration thus mimics two similar submicron junctions separated by an approximately micron-long RuO_2 NW segment. Consequently, the temperature behavior of R_c can be well described by the FIT model (see below).

3.1. Case I: RuO_2 NW devices with $R \approx 2R_c$

We first focus on the case of high-resistance contacts, where $R \approx 2R_c$. The variation of $\log R$ with T^{-1} for the same NW device shown in figure 2(a) is replotted in the inset. This inset indicates that the simple thermally activated conduction (the straight solid line) is only responsible near room temperatures. As the temperature reduces from room temperature, the resistance does not increase as fast as would be expected from the thermal activation process. At liquid-helium temperatures, the resistance approaches a constant, i.e., being barely dependent on temperature. This temperature independent behavior at low temperatures markedly signifies a charge conduction mechanism characteristic of simple elastic tunneling. (It should be noted that this 'saturation' behavior is not due to electron heating.) Quantitatively, the overall temperature behavior of the contact resistance can be well interpreted in terms of the FIT model proposed by Sheng and co-workers [11, 12]. In that model, in addition to the externally applied bias voltage, V_a, the effect of the thermal noise, V_{th}, on the current tunneling is considered. In particular, it is realized that a noticeable V_{th} ($\approx \sqrt{k_B T/C}$, where k_B is the Boltzmann constant) could arise from a tiny capacitance C associated with a *small* tunnel junction formed between two *large* metallic grains. The superposition of this V_{th} (of random sign) with V_a could significantly modify the charge transport properties of the junction.

According to Sheng and co-workers [11, 12], the temperature dependent resistance (for small applied electric fields) across a single small junction is given by

$$R(T) = R_\infty \exp\left(\frac{T_1}{T_0 + T}\right), \tag{1}$$

where R_∞ is a parameter which depends only weakly on temperature, and T_1 and T_0 are characteristic temperatures defined as

$$T_1 = \frac{8\varepsilon_0}{e^2 k_B}\left(\frac{A V_0^2}{w}\right), \tag{2}$$

and

$$T_0 = \frac{16\varepsilon_0 \hbar}{\pi (2m)^{1/2} e^2 k_B}\left(\frac{A V_0^{3/2}}{w^2}\right), \tag{3}$$

where ε_0 is the permittivity of vacuum, $2\pi\hbar$ is Planck's constant, and m is the electronic mass. In equation (1), T_1 can be regarded as a measure of the energy required for an electron to cross the barrier, and T_0 is the temperature well below which thermal fluctuation effects become insignificant. In the derivation of equation (1), the conduction was first modeled [11, 12] as the tunneling of electrons through a single potential barrier of width w, height V_0, and junction area A, where A is given by the size at the point of the two large conducting regions' closest approach. If A is small enough, it was found [11, 12] that the potential barrier seen by the electrons could be effectively narrowed and lowered by the V_{th}. Such a potential-barrier modulation effect greatly influences the tunneling probability, and consequently introduces a characteristic temperature behavior to the normally temperature independent tunneling conductivity (i.e., the elastic tunneling regime). Finally, at sufficiently high temperatures ($T \gg T_0$), the charge transport behavior should cross over to that of thermal activation conduction. To deal with the case of granular composites of macroscopic sizes, it was then shown [12], via the effective-medium theory, that in a network of independently fluctuating tunnel junctions with different values of T_1 and T_0, the conductivity of the network could still be described in terms of a single junction with a representative set of T_1 and T_0.

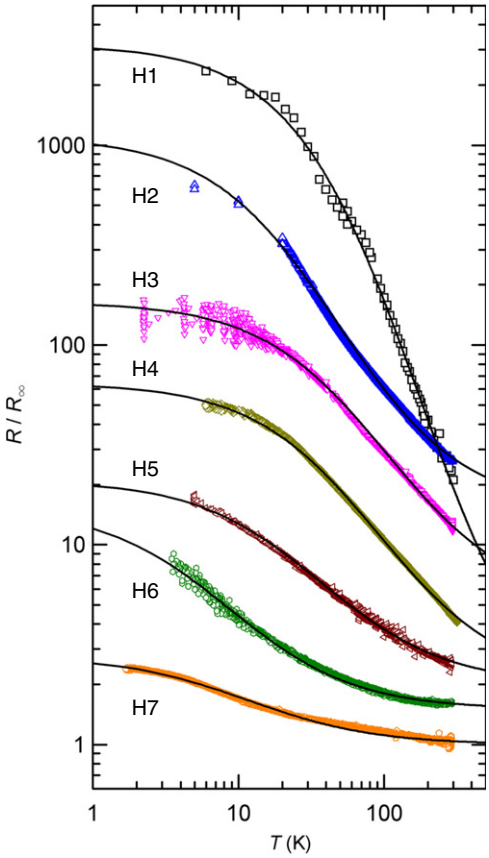

Figure 3. Double logarithmic plot of the normalized two-probe resistance, $R(T)/R_\infty$, versus temperature for seven RuO_2 NW devices, as indicated. The symbols are the experimental data and the solid curves are the least-squares fits to equation (1). For clarity, the results for devices H2, H3, H4, H5, and H6 have been multiplied by a factor of 15, 5, 2, 2, and 1.5, respectively.

Figure 3 shows a plot of our experimental results in double logarithmic scales for seven NW devices having high contact resistances (i.e., $R \approx 2R_c$). The symbols are the experimental data and the solid curves are the least-squares fits to equation (1), with R_∞, T_1 and T_0 as the adjusting parameters. Figure 3 illustrates that equation (1) can well describe the overall temperature behavior for a *wide* range

of temperature between 300 and 1 K. The values of T_1 and T_0 are then extracted. Furthermore, by using SEM and/or AFM, the diameter of the NW and the width of the contacting submicron Cr/Au electrode can be determined, and hence the area of contact A (given by the product of these two quantities) is known. Then, from equations (2) and (3), the values of w and V_0 can be inferred. Our experimental values of the relevant parameters are listed in table 1, where the samples are numbered in sequence with decreasing T_1/T_0. According to equations (2) and (3), the ratio $T_1/T_0 \propto wV_0^{1/2}$. As defined in the FIT model, this ratio can be rewritten as $T_1/T_0 \propto w/\xi$, where $\xi = \hbar/\sqrt{2mV_0}$ is the decay length of the tunneling electron wavefunction inside the barrier. Therefore, a larger ratio T_1/T_0 implies a lower electron tunneling probability (and hence, corresponding to a stronger temperature behavior of R_c).

It should be noted that, in the FIT model, because the two conducting regions remain large in size, the charging energy E_c needed to transfer an electron from one conducting region to the other is completely negligible, i.e., $E_c \ll k_BT$. This situation is distinct from that in the case of Coulomb blockade where, for example, fine metal grains are involved and the charging energy E_c ($\gg k_BT$) rather than the thermal voltage fluctuations plays an essential role in controlling the electronic transport properties. In the present work, the typical volume of our NWs is $\sim$100 nm $\times$ 100 nm $\times$ 1 μm, which is notably larger than the typical sizes of the fine metal grains ($\sim 10^3$ nm^3) used in Coulomb blockade studies [18]. Thus, our NW can be envisioned as a large conducting region separated by an insulating layer from another large conducting region (the submicron Cr/Au electrode) with a junction area A typically of $\sim 100 \times 500$ nm^2. Such a size of A is already small enough to render V_{th} important.

Previously, the FIT model has been successfully applied to explain the temperature behavior of the resistances in various materials, including carbon polyvinylchloride composites [11, 19, 20], polymer composites [21], heavily doped conducting polyacetylene [22], K_xC_{70} thin films [23], and tin-doped indium oxide thin films [24]. In those *macroscopic* composite systems, a very large number of tunnel junctions with usually barely known junction properties were involved. In contrast, the situation is greatly simplified in our case. That is, in our two-probe NW devices, we deal with only two electronic contacts having similar junction parameters, with the junction area A being known. Interestingly, our experimental values of w and V_0 (see table 1) are on the same orders of magnitude to those derived from the representative set of T_1 and T_0 obtained in carbon polyvinylchloride composites [11, 19, 20]. This coincidence may reflect the fact that the sizes of our NWs are approximately the same as the mean size of the conducting chains found in those composites.

The fitted values of w in table 1 seem to be large. However, these values will be reduced by the thermal voltage fluctuations (as well as by the externally applied electric field), according to the FIT theory [11, 12]. On the other hand, the fitted values of V_0 are small. This has recently been proposed to be due to tunneling through *very narrow* channels of width slightly smaller than one half the electron Fermi wavelength [16]. We notice in passing that, if the effective junction area is somewhat reduced from the maximum possible area A defined above, our inferred values of w (V_0) would be slightly decreased (increased) from those values listed in table 1.[4] For instance, if A is reduced by a factor of 5, the value of w would approximately decrease by 30%, while the value of V_0 would approximately double. We also notice that, in this work, the measured R_c cannot be described by the variable-range-hopping [26] conduction form, $R_c(T) = R^*_\infty \exp(T^*/T)^{1/n}$, either with $n = 2$, 3, or 4, where R^*_∞ is a resistance parameter and T^* is a characteristic temperature.

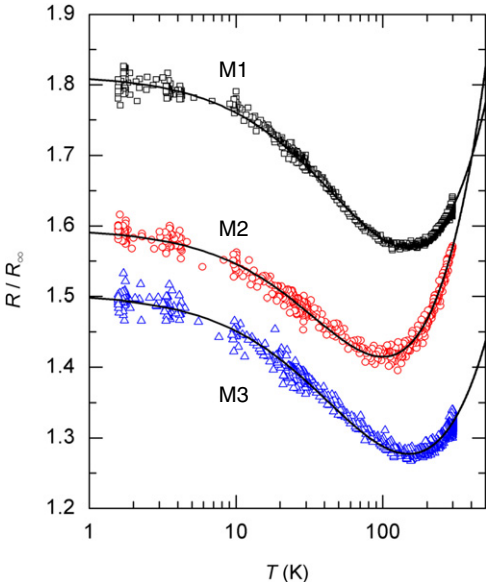

Figure 4. Normalized two-probe resistance, $R(T)/R_\infty$, as a function of the logarithm of temperature for three RuO_2 NW devices, as indicated. The symbols are the experimental data and the solid curves are the least-squares fits to equation (4). For clarity, the result for the M1 device is shifted upward by 0.2.

3.2. *Case II: RuO_2 NW devices with $R = 2R_c + R_s$*

We now turn to the contact resistances showing a temperature behavior as that depicted in figure 2(b). In this case, the value of R_c is comparable with that of R_s, and we may write [27]

$$R(T) = R_\infty \exp\left(\frac{T_1}{T_0 + T}\right) + \alpha T, \qquad (4)$$

where α is a constant. The second term approximates the temperature behavior of resistance for the RuO_2 NWs around room temperatures [17]. As the temperature decreases, the FIT term progressively becomes important, leading to a minimum in the total resistance, R_{min}. Figure 4 shows the measured resistance as a function of temperature for three two-probe devices belonging to this category. The symbols are the experimental data and the solid curves are the theoretical predictions of equation (4). Our fitted values of R_∞, T_1, T_0,

[4] Notice that in the problem of a macroscopic electrical contact, due to the rough and fractal nature of the surface, the real contact (junction) area could be much smaller than (sometimes, even as small as only $\sim$1% of) the apparent contact area [25].

and α, together with other relevant parameters, are listed in table 2. Notice that these values of α are in line with those extracted from the four-probe method[5].

It is worth noting that the different temperature behaviors for case I (figure 3) and case II (figure 4) may be essentially categorized by the low temperature specific contact resistivity defined by $\rho_{c0} = \rho_c(T \to 0)$. Electronic contacts belonging to case I possess $\rho_{c0} \gtrsim 1$ kΩ μm^2 or larger (table 1) while electronic contacts belonging to case II possess $\rho_{c0} \ll 1$ kΩ μm^2 (table 2). Generally speaking, a larger ρ_{c0} reflects a larger potential barrier.

We should mention that the resistance rise with decreasing temperature seen in figure 4 is not due to the weak-localization or electron–electron interaction effects in the presence of disorder [28]. Our RuO_2 NWs are single crystalline and three dimensional with respect to these two quantum-interference effects. As is evidenced in figure 2(c), these two effects only cause a negligibly small resistance rise ($(R - R_{min})/R_{min} \lesssim 0.01$) in our RuO_2 NWs [17].

3.3. Electronic contacts to IrO_2 and Sn-doped In_2O_{3-x} NWs

We further check the validity of the FIT model with other metallic NWs. In addition to RuO_2 NWs, we have fabricated two-probe devices from individual IrO_2 and Sn-doped In_2O_{3-x} (ITO) NWs. Both IrO_2 and ITO are known to exhibit metallic behavior with resistivities comparable with those of normal metals [9, 10, 29, 30]. (The room-temperature resistivities of our IrO_2 and ITO NWs considered here are $\sim$250 $\mu\Omega$ cm.) The IrO_2 NWs were synthesized by the metal–organic chemical vapor deposition (MOCVD) method as described previously [29], while the ITO NWs were grown by the same thermal evaporation method as for the RuO_2 NWs [31]. Material characterizations indicate that these NWs are single crystalline. The temperature behaviors of the NW contact resistances as determined from the two-probe method are shown in figure 5 for one IrO_2 device and one ITO NW device. The symbols are the experimental data and the solid curves are the theoretical predictions of equation (1). The fitted values of the relevant parameters are listed in table 3. Clearly, the FIT model can well describe these two NW devices. This observation, together with that found in the case of RuO_2 NW devices, demonstrates the wide applicability of the FIT model.

In the case of IrO_2 NW devices, however, the temperature behavior of R_c is more complex than that in the RuO_2 NW devices. We have previously found that the surfaces of our MOCVD grown IrO_2 NWs were often fairly inhomogeneous and granular [29]. Therefore, after the fabrication of submicron Cr/Au electrodes, the charge transport through the contacts might reveal a hopping [29, 32] behavior given by $R_c \propto \exp(T^*/T)^{1/2}$. On the other hand, FIT behavior such as that shown in figure 5 has also been occasionally observed. In the latter, it is conceived that the insulating layer at the IrO_2/Cr/Au interface was more or less continuous rather than granular, thus forming a small tunnel junction responsible for the FIT conduction. The different temperature behaviors of R_c for the thermal evaporation grown RuO_2 NWs (where the FIT model mostly applies) and the MOCVD grown IrO_2 NWs (where the FIT model may or may not apply) clearly suggest that electronic contact to metallic nanostructures is a subtle issue which deserves further investigations.

[5] These values of α correspond to $d\rho_s/dT = 0.64$, 1.31, and 0.79 $\mu\Omega$ cm K^{-1} for devices M1, M2, and M3, respectively, where ρ_s is the NW resistivity determined from the four-probe method.

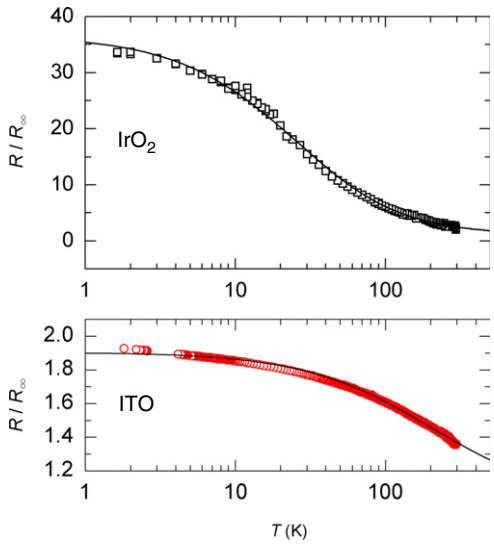

Figure 5. Normalized two-probe resistance, $R(T)/R_\infty$, as a function of temperature for one IrO_2 device and one ITO NW device. The symbols are the experimental data and the solid curves are the least-squares fits to equation (1).

4. Conclusion

We have measured the temperature dependent resistances of individual metallic RuO_2, IrO_2 and ITO NW devices, using the two-probe method, complemented with the four-probe method. By utilizing the two-probe method, we have quantitatively characterized the electronic contacts formed at the interfaces between individual NWs and the submicron Cr/Au electrodes. We found that the overall temperature behavior of the contact resistances can be satisfactorily explained in terms of the thermal fluctuation-induced tunneling conduction process. The relevant junction parameters such as the barrier width and height have been inferred. This work demonstrates that, under appropriate conditions, the charge transport process through an insulating electronic contact between an interconnect and a metallic nanodevice can be fairly well understood.

At low temperatures, the resistance calculated in the FIT theory, equation (1), exactly reduces to the expression expected for simple elastic tunneling, giving rise to a constant resistance as experimentally observed. However, our extracted width of the potential barrier w seems to be relatively large (of several nanometers) in a number of cases. This question, being partly due to an overestimated contact area, requires further theoretical and experimental clarifications. Furthermore, studies of the current–voltage characteristics at high bias voltages, where nonlinear behavior should be important, would be very useful for understanding the nature of (e.g., elastic or inelastic) electron tunneling through the barrier.

Microscopically, the FIT theory has recently been generalized to the case of very narrow conducting channels (e.g., chains of metallic atoms), where the channel width is less than one half the Fermi wavelength [16]. It is predicted that tunneling can occur with a relatively small barrier height, and the inferred value of the barrier width would be only approximately 1 nm.

Acknowledgments

The authors are grateful to Ping Sheng, Hang Xie and Sheng-Shiuan Yeh for valuable discussions. This work was supported by the Taiwan National Science Council through Grant Nos NSC 95-2120-M-009-002 and NSC 96-2112-M-009-025, and by the MOE ATU Program.

References

[1] Lin J F, Bird J P, He Z, Bennett P A and Smith D J 2004 *Appl. Phys. Lett.* **85** 281
[2] Lu W and Lieber C M 2006 *J. Phys. D: Appl. Phys.* **39** R387
[3] Appenzeller J, Martel R, Avouris P, Stahl H and Lengeler B 2001 *Appl. Phys. Lett.* **78** 3313
[4] Lan C, Srisungsitthisunti P, Amama P B, Fisher T S, Xu X and Reifenberger R G 2008 *Nanotechnology* **19** 125703
[5] Gu G, Burghard M, Kim G T, Düsberg G S, Chiu P W, Krstic V, Roth S and Han W Q 2001 *J. Appl. Phys.* **90** 5747
[6] Lin Y F, Jian W B, Wang C P, Suen Y W, Wu Z Y, Chen F R, Kai J J and Lin J J 2007 *Appl. Phys. Lett.* **90** 223117
[7] De Marzi G, Iacopino D, Quinn A J and Redmond G 2004 *J. Appl. Phys.* **96** 3458
[8] Langford R M, Wang T X, Thornton M, Heidelberg A, Sheridan J G, Blau W and Leahy R 2006 *J. Vac. Sci. Technol.* B **24** 2306
[9] Ryden W D, Lawson A W and Sartain C C 1970 *Phys. Rev.* B **1** 1494
[10] Lin J J, Huang S M, Lin Y H, Lee T C, Liu H, Zhang X X, Chen R S and Huang Y S 2004 *J. Phys.: Condens. Matter* **16** 8035
[11] Sheng P, Sichel E K and Gittleman J I 1978 *Phys. Rev. Lett.* **40** 1197
[12] Sheng P 1980 *Phys. Rev.* B **21** 2180
[13] Liu Y L, Wu Z Y, Lin K J, Huang J J, Chen F R, Kai J J, Lin Y H, Jian W B and Lin J J 2007 *Appl. Phys. Lett.* **90** 013105
[14] Moodera J S and Mathon G 1999 *J. Magn. Magn. Mater.* **200** 248
[15] Lin Y H, Wang C C and Lin J J 2008 unpublished
[16] Xie H and Sheng P 2008 unpublished
[17] Lin Y H 2007 *PhD Thesis* National Chiao Tung University, Taiwan
[18] Tinkham M, Davidović D, Ralph D C and Black C T 2000 *J. Low Temp. Phys.* **118** 271
[19] Sichel E K, Gittleman J I and Sheng P 1978 *Phys. Rev.* B **18** 5712
[20] Sichel E K, Sheng P, Gittleman J I and Bozowski S 1981 *Phys. Rev.* B **24** 6131
[21] Paschen S, Bussac M N, Zuppiroli L, Minder E and Hilti B 1995 *J. Appl. Phys.* **78** 3230
[22] Nogami Y, Kaneko H, Ito H, Ishiguro T, Sasaki T, Toyota N, Takahashi A and Tsukamoto J 1991 *Phys. Rev.* B **43** 11829
[23] Wang Z H, Dresselhaus M S, Dresselhaus G, Wang K A and Eklund P C 1994 *Phys. Rev.* B **49** 15890
[24] Ederth J, Johnsson P, Niklasson G A, Hoel A, Hultåker A, Heszler P, Granqvist C G, van Doorn A R, Jongerius M J and Burgard D 2003 *Phys. Rev.* B **68** 155410
[25] Kogut L and Komvopoulos K 2003 *J. Appl. Phys.* **94** 3153
[26] Shklovskii B I and Efros A L 1984 *Electronic Properties of Doped Semiconductors* (New York: Springer)
[27] Kaiser A B, Düsberg G and Roth S 1998 *Phys. Rev.* B **57** 1418
[28] Lee P A and Ramakrishnan T V 1985 *Rev. Mod. Phys.* **57** 287
[29] Lin Y H, Sun Y C, Jian W B, Chang H M, Huang Y S and Lin J J 2008 *Nanotechnology* **19** 045711
[30] Chiquito A J, Lanfredi A J C, de Oliveira R F M, Pozzi L P and Leite E R 2007 *Nano Lett.* **7** 1439
[31] Chiu S P, Chuang H F, Chen F R, Kai J J and Lin J J 2008 unpublished
[32] Sheng P, Abeles B and Arie Y 1973 *Phys. Rev. Lett.* **31** 44